Cancer Nanotechnology

RESEARCH Open Access

Magnetohyperthermia-synergistic glioma cancer therapy enabled by magnetic graphene oxide nanoheaters: promising nanostructure for in vitro and in vivo applications

Roghayeh Sheervalilou[1], Samideh Khoei[2,3*], Sepideh Khoee[4], Milad Shirvaliloo[5,6], Elaheh Sadri[3], Sakine Shirvalilou[2,3*] and Mina Goudarzi[7]

*Correspondence: khoei.s@iums.ac.ir; skhoei@gmail.com; sakine.shirvaliloo@gmail.com

[1] Pharmacology Research Center, Zahedan University of Medical Sciences, Zahedan, Iran
[2] Finetech in Medicine Research Center, Iran University of Medical Sciences, 1449614525, Tehran, Iran
[3] Department of Medical Physics, School of Medicine, Iran University of Medical Sciences, 1449614525, Tehran, Iran
[4] Department of Polymer Chemistry, School of Chemistry, College of Science, University of Tehran, Tehran, Iran
[5] Infectious and Tropical Diseases Research Center, Tabriz University of Medical Sciences, Tabriz, Iran
[6] Future Science Group, Unitec House, 2 Albert Place, London N3 1QB, UK
[7] Department of Physiology, School of Medicine, Iran University of Medical Sciences, Tehran, Iran

Abstract

In the present study, a magnetohyperthermia (MH)-based therapy is introduced as an effective treatment for deep-seated tumors especially glioma, which combines the magnetothermal effect and the reactive oxygen species (ROS) induced with magnetic graphene oxide (GOMNPs) nanoheaters to overcome the issue of limited therapeutic efficacy in the current magnetothermal therapeutic strategy. Magnetic graphene oxide nanoheaters with a size of 34 nm and a surface charge of − 35 mV showed very little toxicity under in vitro and ex vivo circumstances based on MTT and hemolysis assay, respectively. The application of GOMNPs under an alternating magnetic coil (AMC) showed that they had high specific absorption rate (SAR, $P < 0.01$), with enhanced level of ROS production within the tumor microenvironment. The results confirmed a significant increase in the SAR in blood compared to culture media ($P < 0.01$), which indicates the improvement of magnetohyperthermia performance in in vivo conditions compared to in vitro. A significant therapeutic efficacy was achieved with a dosage of 30 mg/kg of GOMNPs following 3 therapeutic courses under alternating magnetic field (AMF) compared to AMF alone ($P < 0.05$). GOMNPs exhibited a strong anti-glioma effect by inhibiting tumor growth, and increasing the survival ratio by inducing apoptotic cell death ($P < 0.05$). The Bax/Bcl2 protein and gene ratio confirmed a higher rate of apoptotic death in the MH-treated group ($P < 0.05$). Combination of magnetohyperthermia with conventional modalities may offer tremendous clinical advantages compared to the currently available methods.

Keywords: Magnetohyperthermia, Glioma, Graphene oxide, Magnetic nanoheaters, Reactive oxygen species, Specific absorption rate

Graphical Abstract

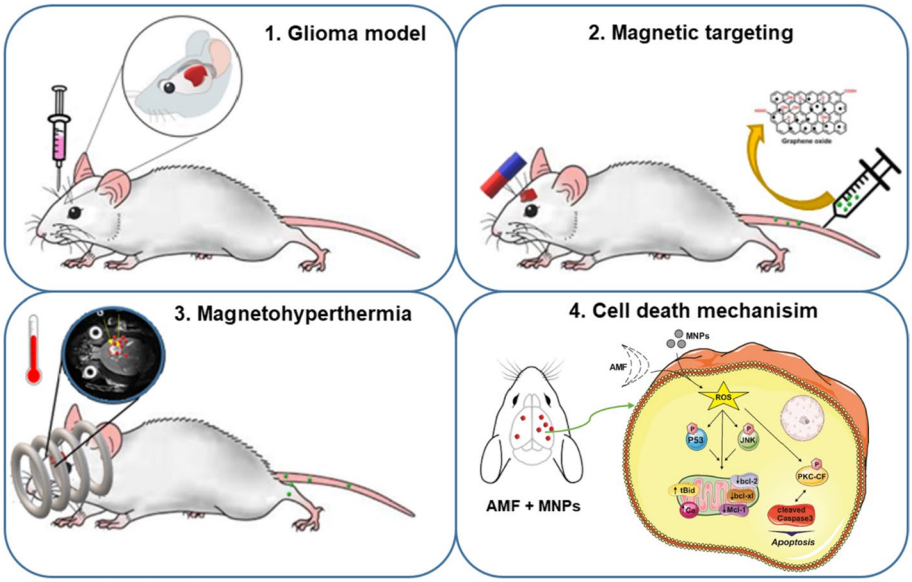

Introduction

The recently developed mode of thermotherapy termed targeted magnetic hyperthermia (TMH) or simply "magnetohyperthermia" (MH) has received considerable attention in recent years for the treatment of deep solid tumors especially brain (Shirvalilou et al. 2021), prostate (Johannsen et al. 2010), colon (de Escalona et al. 2016) and breast cancers (Beola et al. 2018; Hilger et al. 2005). One of the great potentials of MH treatment is non-invasive penetration into deeply located tissues and targeted destruction of cancer cells without damaging the neighboring cells (Liu et al. 2020b). Magnetohyperthermia is the conversion of electromagnetic energy into heat by magnetic nanoparticles (MNPs) which occurs when exposed to alternating magnetic fields (AMF) (Périgo et al. 2015; Rego et al. 2020; Rodrigo et al. 2020). Under an AMF, a local increase in the temperature (40–44 °C) facilitated by nanoparticles is sufficient to inhibit tumor cell growth (Kalamida et al. 2015). In fact, MNPs play the role of energy converters and produce heat as a remote nano-heater due to molecular vibrations (Di Corato et al. 2014; Jahangiri et al. 2021; Piazza et al. 2020). The use of magnetic nanoparticles as a magnetothermal sensitizer was first reported by Gilchrist et al. in 1957 (Gilchrist et al. 1957). Since then, iron oxide nanoparticles (IONPs) have been continuously modified for a variety of nanomedicine-related applications, including targeted drug delivery, magnetic nanoheaters, and MRI contrast agents (Gu et al. 2020; Oghabian et al. 2011).

The main challenge in the case of MH is to generate the required heat for the accumulation of a sufficient amount of MNPs in the tumor site (Kargar et al. 2018; Shaterabadi et al. 2018). It has been shown that SPIONs can be directed at tumor sites by application of external magnetic fields (EMF) and retention (EPR) effect. To this end, iron oxide-based nanoparticles should be stabilized and a way not to agglomerate in

aqueous environments, especially after being exposed to EMF (El-Dek et al. 2018; Gu et al. 2020). When administered in vivo, the aggregation of MNPs often leads to precipitation, resulting in shortening of blood circulation time, hence, the prerequisite of immobilizing nanoparticles (Kumar et al. 2018). To address this issue, we developed a graphene oxide (GO) framework for generation of decorated SPIONs. GO is known to improve the biocompatibility and colloidal stability of Fe_3O_4 (Hatamie et al. 2021; Kumar et al. 2018). Investigations by Jang et al. (2009) and Chen et al. (2013) have confirmed that GO nanosheets with unique physical and chemical properties might enhance antibacterial activity by generating ROS. In addition, the high electrical and thermal conductivity of GO nanosheets may cause a synergistic effect of SAR (specific absorption rate) in combination with Fe_3O_4 (Asadi et al. 2018; Liu et al. 2020b).

In this regard, herein we studied the therapeutic potential of magnetohyperthermia and PLGA-coated GO/SPIO nanoheaters (MNPs) as a theranostic agent. To ensure the colloidal stability and biodistribution on physiological medium, GOSPIONs are frequently functionalized with biocompatible PLGA polymers. In clinical trials, critical challenges in the brain cancer treatment include local hyperthermia and non-invasive remotely controlled therapy. As such, in this study, we tried to use the AMF and magnetic graphene oxide nanoparticles as a theranostic platform for local treatment of brain cancer in vitro (C6 and OLN-96 cells) and in vivo (C6 glioma bearing rats), and MRI contrast agents. For in vivo studies, Wistar rats with glioma were recruited, and GOMNPs were then administered to the rats, along with external permanent magnets (neodymium-iron-boron, 1.3 T). Then, for magnetic hyperthermia, the head was placed inside the coil (13.56 MHz, 40 A/m), and finally, the efficiency of MH treatment was evaluated by following the tumor volume changes and the survival rate of treated rats. Since the classical concept of apoptosis and necrosis occurring independent from one another has already been refuted (Beola et al. 2018), tumor vasculature may collapse and trap the applied heat, and resulting in necrosis or apoptosis (Spirou et al. 2018). Therefore, in this study, the expression levels of Bax and Bcl-2 gene and Bax and Bcl-2 proteins were investigated by real-time PCR and Western blotting method, respectively.

Results

Characterization of the nanoparticles

A summary of the characteristics of the synthesized polymer-coated GOSPIOs nanoparticles is provided in Fig. 1. The fabrication of theranostic GOSPIOs nanoparticles is illustrated schematically in Fig. 1A. As shown in the TEM image, the SPION nanoparticles were almost spherical in shape, while GO nanoparticles exhibited a sheet-like morphology, being decorated with SPIONs on their surface (Fig. 1B). In the image, a good distribution of nanoparticles on the GO nanosheets can be seen. In addition, the morphology of GOSPIOs was investigated through scanning electron microscopy (SEM), and the obtained images confirmed the results of TEM imaging (Fig. 2C). The hydrodynamic size of PLGA-coated GOSPIONs was 74.68 nm (Fig. 1D). The nanoparticles were negatively charged with -36 mV in deionized water. According to previous studies, such value of negative surface charge of nanoparticles (>|-35|) may confer sufficient stability in the aquatic environment (Clogston and Patri 2011; Salopek et al. 1992). The saturation magnetization (SM) of GOSPIONs was measured to be 43.6 emu/g with a very narrow remanent loop, which indicated

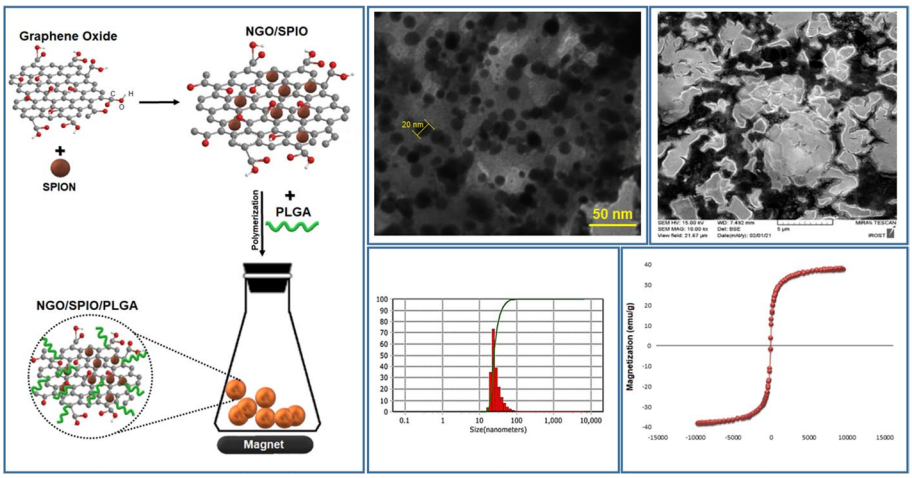

Fig. 1 **A** Schematic illustration of nanoparticle synthesis, **B** TEM of GOSPION nanoparticles where SPION nanoparticle are seen dispersed on GO surface, **C** SEM, **D** particle size, and hysteresis curve of GOSPIONs

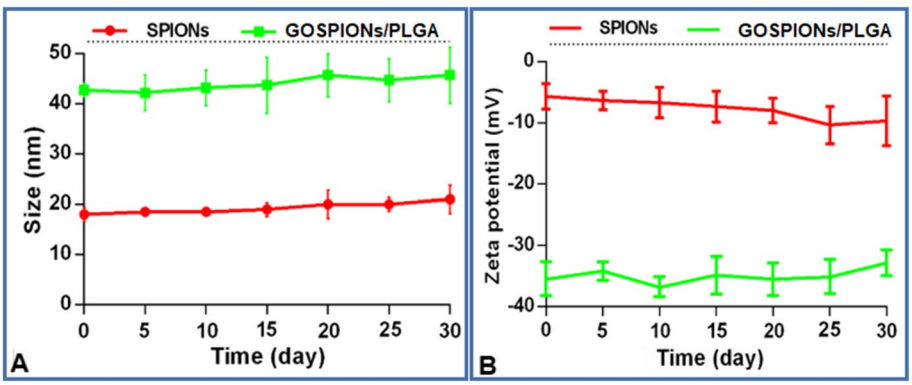

Fig. 2 Changes in **A** size and **B** zeta potential of nanoparticles during 30 days

the superparamagnetic property of polymer-coated magnetic nanoparticles (Fig. 1E). This feature can help to increase the induction of heat through the application of an AMC (Liu et al. 2020b). Hydrodynamic size in a narrow range by DLS measurements was available after 1 month (Fig. 2A). No signs of aggregation and coagulation or sedimentation were seen. The surface charge of nanoparticles also did not show any significant difference during this period of time (Fig. 2B, $P > 0.05$).

Ex vivo results

Permanent magnetic field simulation

In this study, the Teslameter was used to measure the magnetic field flux density as a function of the distance between two magnets (6 cm, Fig. 3A, B). The strength of each magnet was 1.3 T (according to the manufacturer's instructions), while the relative permeability of the 2-dimensional field at the periphery of the magnet was 0.5 T at highest. Using the data obtained from these simulations, a color map and graphs of the resulting magnitudes of the magnetic field density at the indicated locations were created (Fig. 3B, C). The purpose of designing the magnetic field phantom was to choose a configuration

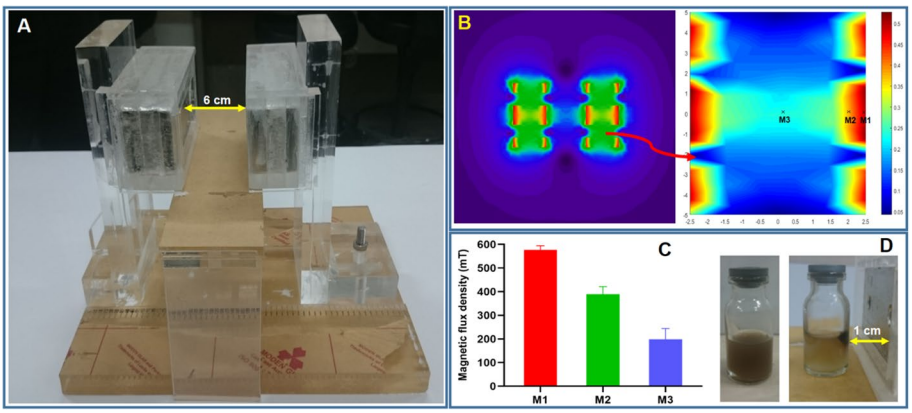

Fig. 3 **A** Magnetic field phantom consisting of two permanent magnets, **B** simulation of permanent magnetic field inside the phantom, **C** magnetic field intensity at different points inside the phantom (M_1, M_2, and M_3), **D** suspension of nanoparticles inside the magnetic field

that would create a narrow region with maximum magnetic intensity and minimum intensity in the surrounding areas for targeted delivery of magnetic nanoparticles. Figure 3D shows the superparamagnetic property of nanoparticles that are completely dispersed in the medium without aggregating after the field is dismissed.

Hemolysis assays of red blood cells

Incubation of rat RBC samples with different concentrations of GOSPIOs was used to evaluate the biocompatibility of nanoparticles in ex vivo conditions (Fig. 4A). Based on the results, nanoparticles at a concentration of 2000 µg/mL show a little hemolysis (≈ 2%), much lower than the allowed level of hemolysis (5%). According to this criterion, GOSPIOs nanoparticles can be safely injected into rat.

AMC simulation and temperature–time curves of GOSPIOs nanoheaters

Figure 4 shows the simulated image of the almost uniform distribution of alternating magnetic field inside the coil (Fig. 4B). To determine the thermomagnetic performance of GOSPIOs nanoheaters, the suspension of different concentrations of nanoparticles (1, 2 and 3 mg/mL) was subjected to the AMC for 10 min and the temperature changes were monitored by an IR camera (Fig. 4C). The temperature–time curves at a power of 80 W during AMF exposure are plotted in Fig. 4D. The heating efficiency of GOSPIOs nanoheaters in an AMC was determined by calculating the SAR value. The SAR calculated from measurements were 174.16 ± 10.5, 195.27 ± 8.45 and 263.02 ± 9.66 W/g Fe, respectively. As the concentration of GOSPIOs nanoparticles increased, the SAR values increased.

The fold-change in the temperature rise rate (TER) of GOSPIOs nanoparticles in different concentrations (1, 2 and 3 mg/mL) compared to the control sample after 10 min exposed with AMF was 3, 6.5, and 12.3-fold, respectively. These results confirmed that SPIONs could efficiently act as magnetic nanoheaters to convert magnetic energy to heat, which makes them suitable as thermal sensitizing agents. ILP is introduced as a thermal conversion capability that allows comparison of SAR values independently of various coil field-dependent parameters (field strength and frequency).

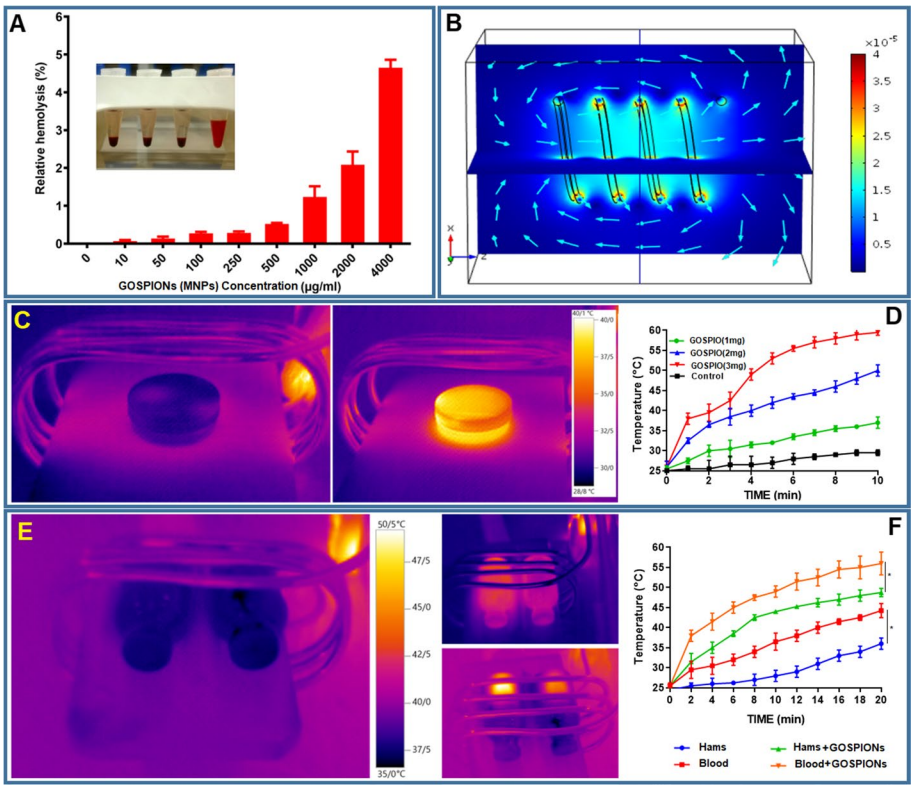

Fig. 4 **A** Ex vivo hemolysis results of the different concentrations of GOSPIONs after incubation (2 h) with diluted red blood cells of rat, **B** simulation of alternating magnetic field inside the coil, **C**, **D** thermometry of different concentrations of GOSPIONs by IR camera during 10 min (**C**: t = 0 and **D**: t = 10 min), **E**, **F** Thermometry of different concentrations of nanoparticle suspension in culture media (Hams) and blood by IR camera during 20 min (**E**: *t* = 0, and **F**: *t* = 20 min)

Table 1 Thermal properties of GOSPIONs nanoparticles exposed to alternating magnetic field (13.56 MHz, 80W)

GOSPION concentration	Time (s)	ΔT (°C)	H (A/m)	f (MHz)	SAR (W/g)	ILP (nHm^2/g)	TER
1 (mg/mL)	600	9	40	13.56	174.16	8	3
2 (mg/mL)	600	18.5	40	13.56	195.27	9	6.5
3 (mg/mL)	600	37	40	13.56	263.02	12.12	12.3

Hence, in addition to the SAR factor, the ILP parameter is also calculated here (Table 1). The results of ILP of different concentrations of nanoparticles show that by increasing the amount of Fe3O4, the value of SAR also increases, since the increase in the iron content of nanoparticles accentuates magnetization and thus increases the value of SAR.

Temperature–time curves of Blood in AMC

To compare the effect of different environments on the extent of temperature changes in cell and animal conditions, suspension of nanoparticles in culture media (Hams-F12)

and blood was used (Fig. 4E). The results of monitoring of temperature changes during 20 min showed that the change in temperature in the blood was significantly higher than the culture medium ($P < 0.05$, Fig. 4F).

In vitro results

Evaluation of GOSPIOs as a MHT nanoheater in vitro

Figure 5A shows the viability rates of OLN-93 and C6 cells treated with different concentrations (0–2 mg/mL) of GOSPIOs in the presence or absence of an AMF. Both cell lines treated with GOSPIOs nanoparticles demonstrated more than 80% viability at concentrations up to 100 µg/mL, while in the presence of the AMF the viability of the cells was greatly reduced ($P < 0.001$), which means that the nanoparticles themselves had no apparent toxicity and were biocompatible. Though, they had a high ability to produce heat in the presence of the AMF. IC_{50} values were calculated for both cell lines treated with nanoparticles with and without AMC application, and the results are reported in Table 1. The IC_{50} values for two healthy and cancer cell lines were not found to significantly differ from one another ($P > 0.05$, Fig. 5B). Meanwhile, the IC_{50} values for the treatment with and without applying the AMC had a significant difference ($P < 0.001$). Somehow, the treatment ratio for both cell lines showed an increase of over 90% by applying the alternating magnetic field (Table 2). The toxicity effect of different therapeutic modalities on C6 cancer cell line is shown in the light microscopic images in Fig. 5C. TEM images of C6 cells in Fig. 5D show the entry of nanoparticles into the cells.

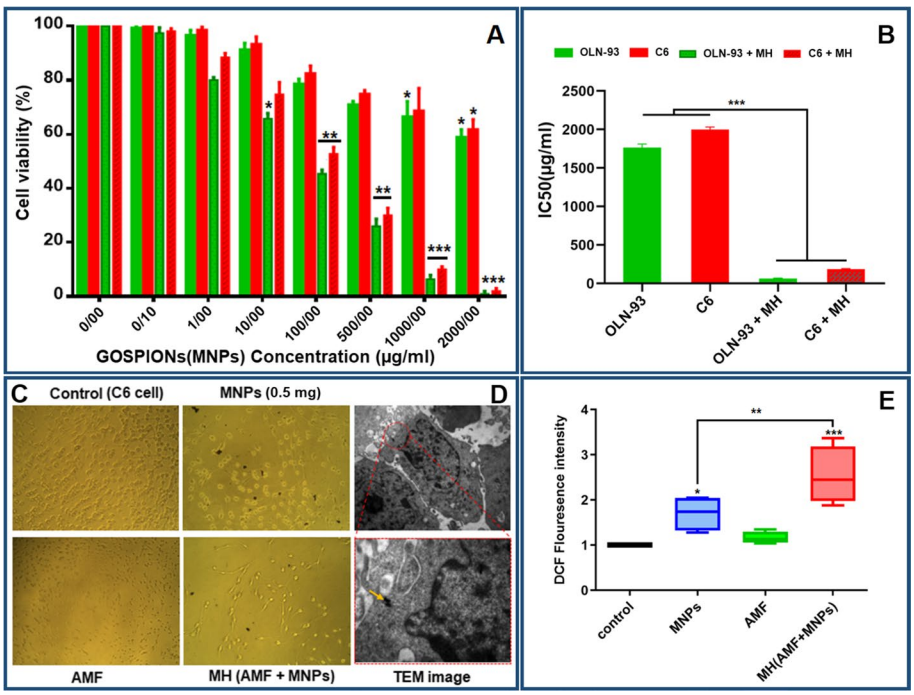

Fig. 5 **A** The toxicity effects of 24 h treatment with MNPs, and MH on C6 and OLN-93 cell lines, **B** IC50 concentration for C6 and OLN-93 cells, **C** optical image of treated C6 cells, **D** TEM image of cells, and **E** ROS concentration produced under different treatments. (Mean ± SD, $n = 3$)

Table 2 IC50 values and therapeutic efficiency of cancer (C6) and normal (OLN-93) cells calculated based on MTT results

Type of cell	IC50 (MNPs)	IC50 (MNPs + AMF)	Therapeutic efficacy (%)
OLN-93 (Normal)	2456	84	96.57
C6 (Glioma)	3182	113	96.44

Intracellular ROS measurement

ROS concentration in C6 cells was analyzed to determine the effect of nanoparticles and magnetic hyperthermia on ROS generation. As can be seen in Fig. 5E, GOSPIOs and MH led to higher levels of intracellular ROS ($P<0.05$). The results showed that GOSPIOs in combination with AMF could improve the AMF effects by increasing the ROS generation in C6 cells.

Apoptosis cell death assessment

Annexin V-FITC/PI flowcytometry assay was used to investigate cell death in the treatment of magnetic hyperthermia and evaluate the rate of apoptotic and necrotic cell death. Figure 6A shows the fluorescence microscopic images of both C6 and OLN-93 cells treated with GOSPIOs alone or in combination with AMF. When cells were treated with GOSPIOs or AMF alone, the treatment effect on viable cells was less pronounced (Fig. 6B). However, magnetic hyperthermia treatment at 43 °C showed a high degree of apoptosis compared to single treatment groups ($P<0.01$, Fig. 6B). The results of flow cytometry, like the MTT test, did not show a significant difference between the death of healthy and cancer cell lines ($P>0.05$, Fig. 6B).

In vivo results

Heating profile and thermal dose calculation of AMC coil

For magnetic hyperthermia, after intravenous injection of GOSPIOs nanoparticles, the glioma-bearing rats were placed inside the coil (Fig. 7A, B, 30W) by head. The temperature changes of the rats were measured by IR camera and thermocouple, and the temperature–time graph is shown in Fig. 7C. The recorded temperature changes between the IR camera and the thermocouple did not record a significant difference (±0.85 °C, $P>0.05$, Fig. 7D). The presence of GOSPIOs caused a significant increase in temperature compared to the AMC alone ($P<0.05$). Without the presence of nanoparticles, the increase in temperature was not local and reached a therapeutic temperature of 43 degrees in a longer period of time. The temperature initially rose rapidly in the head until it reached 41 °C at 2 min, and after temperature expansion, the temperature slowly increased to 44 °C during the remainder of the treatment process. According to the results of thermometry for hyperthermia at 43–44 °C, rats were placed in AMC for 26 min for AMF treatment alone and 12 min for MH treatment (Fig. 7D). These results clearly showed the suitability of these magnetic nano-heaters for anti-cancer magnetic hyperthermia therapy. To compare the thermal dose received by rats in the presence and absence of GOSPIOs, CEM 43 °C was calculated for both positions at 2 and 12 min based on the thermometric data of Fig. 7C. The CEM 43 °C for rats treated with AMF

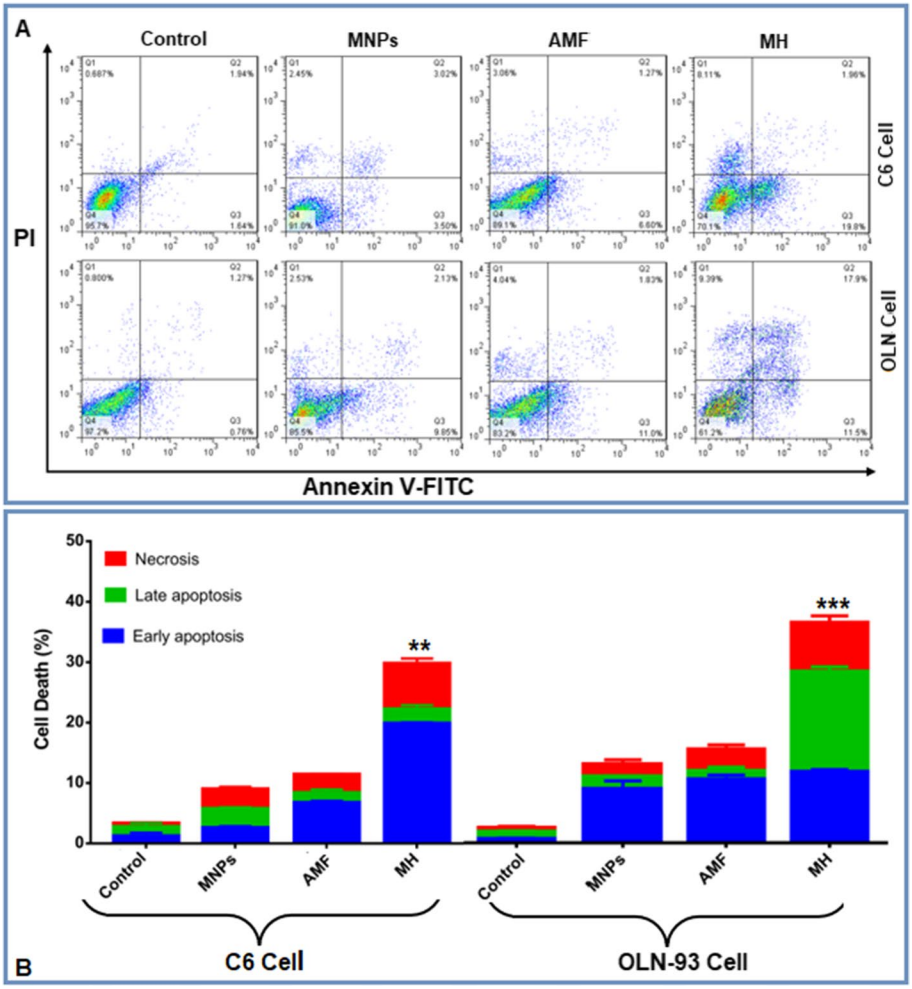

Fig. 6 The Annexin-V/PI assay for evaluating the apoptosis of C6 and OLN-93 cells, **B** the percentage of apoptotic and necrotic cells, 24 h after treatment with MNPs (GOSPIONs) and AMF only or combined with AMF exposure (MH). (Mean ± SD, $n = 3$, (*) $P < 0.05$, (**) $P < 0.01$ and (***) for $P < 0.001$, respectively)

without nanoparticles after 2 and 12 min of were equal to 0.00048, and 0.3419 min, respectively. In contrast, these values increased significantly to 0.0312 and 69.125 min for MH treatment, respectively ($P < 0.05$).

Liver enzyme assay

Abnormal liver enzyme levels may signal liver damage. Upregulation of Alanine amino transferase (ALT) and Aspartate amino transferase (AST) in the serum secondary to leakage from hepatic cells is increased in liver damage (Giannini et al. 2005). AST and ALT are thought to be good indicators of hepatic damage. Our results showed that there is no significant difference between the treatment and saline (control) groups in terms of ALT activity ($P > 0.05$, Fig. 7E). AST concentrations increased in the MH group treated with nanoparticles (GOSPIONs) and AMF ($P < 0.05$). However, there were no significant changes in the level of AST in the GOSPIONs or AMF groups in comparison with the saline group ($p > 0.05$).

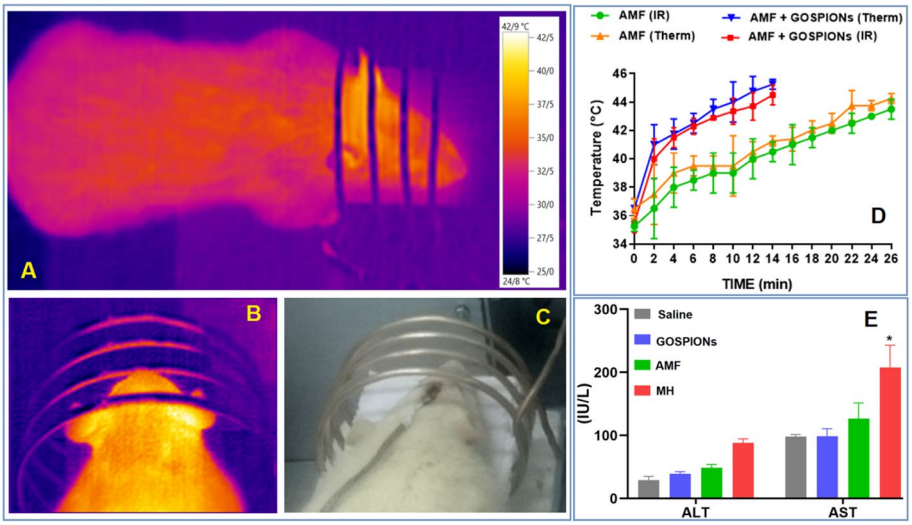

Fig. 7 Nanoparticles as an effective in vivo heat mediator under AMF. **A**, **B** Infrared camera images of the glioma rat during 26 min of hyperthermia, **C** the position of the rat inside the coil, **D** temperature variations profile of glioma tumor-bearing rat treated with intravenous injection of nanoparticles in the presence of AMF (13.56 MHz, 40 A/m, 26 min) as a function of time. Thermometric results are recorded by thermocouple and IR camera, **E** serum level activity of AST&ALT in glioma rats treated with nanoparticles (GOSPIONs), AMF and MH (GOSPIONs + AMF)

In vivo magnetic hyperthermia efficacy via MRI assay, tumor volume and survival rate

The antitumor efficiency of the different treatment modalities (GOSPIONs, AMF and magnetic hyperthermia (GOSPIONs + AMF) were evaluated in rat glioma-bearing tumor by monitoring tumor volume and survival time (Fig. 8). On the 13th day after cell implantation in the brain of test subjects, T2-weighted MR imaging was used to confirm tumor formation. In addition, on the 28th day, rats in different treatment groups were photographed again to check the changes in the tumor volume for monitoring the therapeutic process. Figure 8A shows the healthy brain and the brain of treated rats after 14 days of treatment. The images show a significant increase in the tumor volume with a big tumor mass in the control group. The graph of tumor volume changes for surviving rats in different groups according to MRI image data is plotted in Fig. 8B. In the treatment group of AMF and magnetic hyperthermia (MH), a significant difference can be seen in the control of tumor growth compared to the control group until the 28th day ($P < 0.05$). If after the 28th day, we observed an increase in tumor volume in the AMF alone group. Magnetic hyperthermia also showed tumor inhibition until the 42nd day (Fig. 8B). The survival rate was found to increase until the 70th day after the first tumor therapy (Fig. 8C). Death following this period could be due to tumor recurrence, which can be seen in the curve of tumor volume changes. However, there was no significant difference between GOSPIOs and AMF alone ($p > 0.05$), which suggests a key role for nanoparticles in local temperature rise in hyperthermic treatment, which in this case has led to a significant increase in the treatment efficiency ($P < 0.01$).

Molecular study via real-time PCR assay and Western blotting

Our in vitro results revealed that heat treatment at 43–44 °C induced cell apoptosis and inhibits the proliferation of C6 and OLN-93 cells. According to this, under in vivo

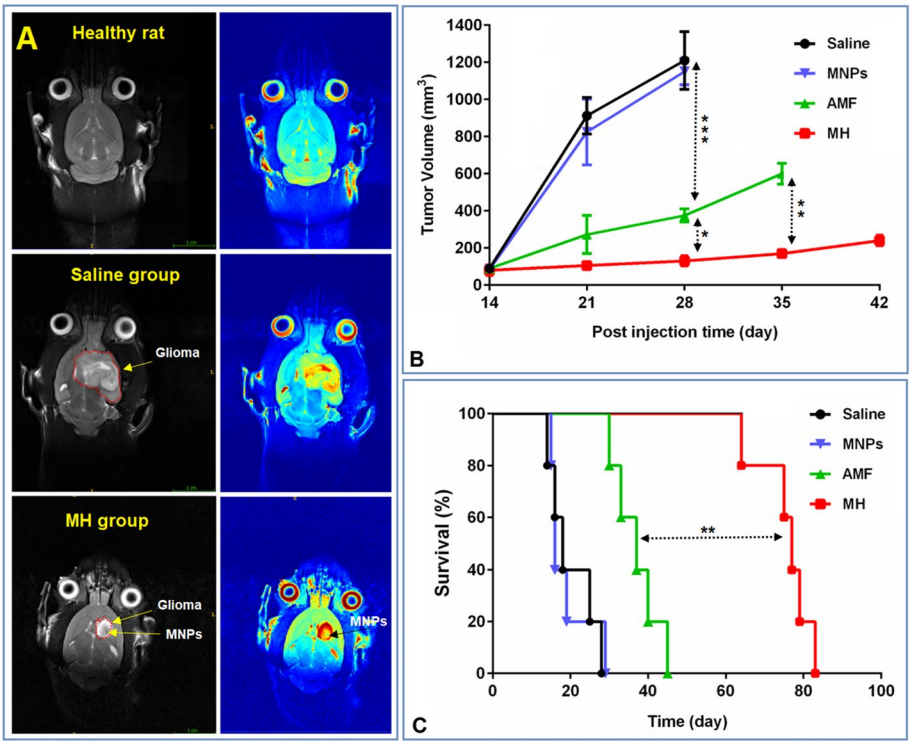

Fig. 8 **A** Axial T2-weighted images of C6 glioma bearing rats obtained for different treatment groups (saline and MH), **B** Glioma tumor volume in different treatment groups (saline, GOSPIONs, AMF, MH) up to the 42th day, **C** percentage of survival time for different treatment groups (Kaplan — Meier plot)

conditions, the expression of genes and proteins related to apoptosis was analyzed as an indicator of death. One hour after applying the last fraction of hyperthermia, 3 rats in each group were sacrificed and their tumor tissues were extracted for molecular tests. Considering that, an apoptosis signaling pathway including the activation of cancer cells is associated with a significant increase in Bax protein expression level and Bcl-2 suppression, therefore, Bax and Bcl-2 gene and protein expressions by real-time PCR and Western blotting were evaluated, respectively. As inferred from the examination of tumor volume changes and survival rates of rats (Fig. 8) treated with GOSPIOs nanoparticles, these rats showed almost no Bax or Bcl-2 gene (Fig. 9) or protein expression (Fig. 10). Rat glioma tissue treated with AMF process showed a higher value of Bax expression compared to the control and nanoparticle-treated groups, indicating a stronger regulatory effect on apoptosis in the treated group (Figs. 9 and 10). The value of Bax/Bcl-2 ratio in both AMF- and MH-treated groups was ≥ 1, which means that the tumor cells have undergone apoptosis significantly. Treating rats with the magnetic hyperthermia revealed a significantly higher Bax gene and protein production than other groups ($P < 0.01$), whereas the Bcl-2 levels showed a slight decrease (Figs. 9 and 10). Ultimately, the present study detected a stronger increase in Bax/Bcl-2 gene and protein ratio, after combinatorial therapy of AMF plus GOSPIOs nanoheaters ($P < 0.001$, $6 > \text{ratio} > 3$, Figs. 9 and 10) was applied.

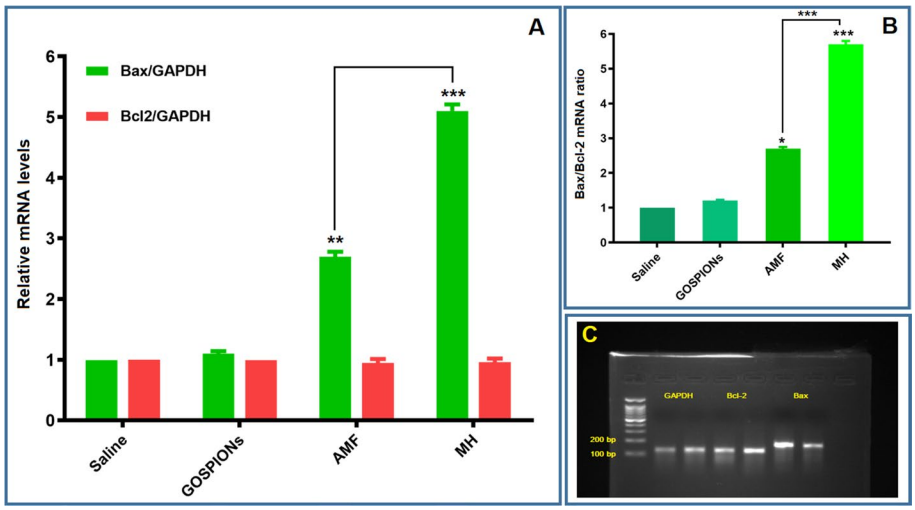

Fig. 9 **A** Relative mRNA expression of Bax and Bcl-2 genes in glioma tumor tissue 24 h after treatment with various therapies (saline, GOSPIONs, AMF, MH), **B** apoptotic index pattern at the mRNA level after treatments (Bax/Bcl-2 ratio), **C** electrophoresis of real-time PCR-amplified products [mean ± SD, $n = 3$, (*) $P < 0.001$]

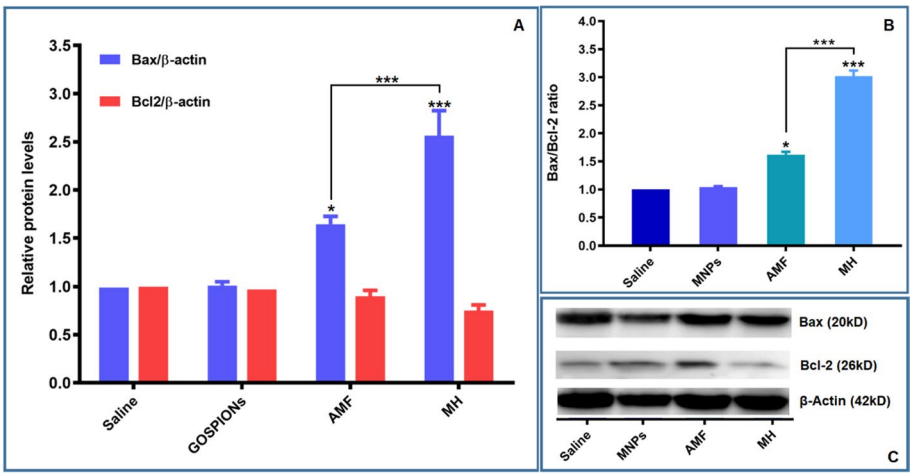

Fig. 10 **A** Effects of Saline, GOSPIONs, AMF, MH on relative protein expression of Bax and Bcl-2, **B** apoptotic index pattern at the protein level after treatments (Bax/Bcl-2 ratio), and **C** protein expression detected by Western blot [mean ± SD, $n = 3$, (*) $P < 0.001$]

Discussion

In the present study, the efficacy of MHT in the treatment of glioblastoma was investigated on monolayer cultures and a murine model of glioma based on functional and structural evaluation to achieve the best treatment efficacy. Therefore, here we measured many key effective parameters on MHT, including characteristics such as size, shape, surface charge, coating, colloidal stability, magnetic properties and concentration of GOSPIO nanoparticles to be used as nanoheaters (Belanova et al. 2018; Karimipour et al. 2021; Vilas-Boas et al. 2020). The synthesized nanoparticles with a size of 42 nm and a surface charge of − 36 mV (anionic) showed good stability in 30 days without agglomerations, and by keeping the size below 50 nm, which can be suitable for cell

and animal studies (Figs. 1, 2). The results of many studies in targeted delivery such as Iyer et al. and Bychkova et al. have proven that nanoparticles with a size > 200 nm are quickly absorbed by the reticuloendothelial system (RES) and accumulated in the liver and spleen, and nanoparticles < 6 nm are excreted by the kidneys (Bychkova et al. 2012; Iyer et al. 2006). On the other hand, due to the structural difference between the vasculature of normal tissue and tumor tissue, nanoparticles > 10 nm can easily enter the tumor tissue, but slow venous return and low lymphatic clearance keep MNPs in the tumor site, which is due to EPR (Greish 2010; Lanier et al. 2019). In addition to the size, the surface charge of nanoparticles also affects the circulation of nanoparticles. Cationic nanoparticles are likely to be removed by the RES upon binding blood proteins (protein corona effect) or undergoing an increase in size (Shirvalilou et al. 2020; Zeng et al. 2019). Another effective factor on the heating features is the stability and superparamagnetic properties of nanoparticles. As Youhannayee et al. and Umar et al. also showed, coating magnetic nanoparticles and loading them on graphene oxide sheets can prevent nanoparticles from aggregating even after applying an external magnetic field (Umar et al. 2020; Youhannayee et al. 2019). In this study, we used these two methods to increase the stability of superparamagnetic nanoparticles, also we used PLGA polymer for coating and graphene oxide sheets to increase the stability of GOSPIO nanoparticles. Another characteristic of nanoparticles with critical importance in MH therapy is the SAR parameter (Umar et al. 2020). Tong et al. demonstrated that although the SAR increases with the size of Fe nanoparticles, it is typically in the critical superparamagnetic size range of 25–26 nm (Tong et al. 2017). Due to the dependence of SAR on parameters such as the frequency and strength of the applied magnetic field, in some references, the ILP parameter has also been used instead of SAR (Li et al. 2015; Xu and Pan 2019). Here, we calculated both parameters, and the results clearly indicated an increase in SAR or ILP with increasing concentration of GOSPIO nanoparticles and as well as hyperthermia time (Table 3). In our study, magnetic hyperthermia treatment was performed at a field intensity of 40 A/m. SAR, ILP and TER calculated from thermal measurements for 3 mg/mL of GOSPIO nanoparticle (containing 0.98 mg/mL Fe) were 263.02 W/g_{Fe}, 12.12 nHm^2/g and 12.3, respectively. Jeon et al. reported that PEG-coated iron oxide nanoparticles not only improved in vivo stability but also improved heating when Fe_3O_4 was exposed to AMC at high H and f (Jeon et al. 2020).

In recent studies, researchers like Umar et al. and Liu et al. have reported that graphene magnetic nanoparticles can perform better inside the magnetic coil than iron nanoparticles, and also ensuring better SAR at intracellular tumor (Liu et al. 2020a; Umar et al. 2021). In fact, GO can significantly increase the dielectric loss and thermal conductivity due to its good electronic and thermal conductivity, which ultimately leads

Table 3 Primer sequences used for real-time PCR

Gene	Forward primer (5′-3′)	Reverse primer (5′-3′)	Amplicon length (bp)
Bax	CGATGAACTGGACAACAACATGG	GCAAAGTAGAAAAGGGCAACCAC	150
Bcl-2	TGGATGACTGAGTACCTGAA	GAGACAGCCAGGAGAAATCAAA	124
GAPDH	AGTTCAACGGCACAGTCAAG	TACTCAGCACCAGCATCACC	118

to an increase in SAR (Eivazzadeh-Keihan et al. 2022; Liu et al. 2012; Sugumaran et al. 2019), suggesting that our synthesized nanoparticles had high magneto-thermal sensitizer potential. Figure 4E indicates that these nanoparticles can play a more effective role as AMC nanoheaters in in vivo circumstances than in vitro because the blood as an "iron pool" contains iron molecular ions (hemoglobin), which enhances the heating effect (Berkovitch et al. 2000; Périgo et al. 2015).

For biomedical application, the toxicity of nanoparticles was first investigated by MTT test and hemolysis. MTT and hemolysis assays showed that the cytotoxicity of GOSPIONs in concentrations near 1 mg/mL was negligible (Figs. 4A and 5A). While the application of AMF in the presence of GOSPIONs showed high toxicity for both cell lines (Fig. 5A–C). The results clearly demonstrated that GOSPIONs had high magnetic heating potential, and significantly decreased the viability of cells ($P < 0.01$). But there was no significant difference between healthy (OLN-93) and cancer (C6) cells treated ($p > 0.05$). Although some researchers such as Oei et al. have shown that normal cells are less sensitive to hyperthermia than cancer cells (Mohammadi et al. 2012; Oei et al. 2017), in contrast, researchers such as Roizin-Towle and Pirro (1991) and Dewey et al. (1977) argue that the major disadvantage of hyperthermia is that, in general, normal and malignant cells have the same sensitivity to heat.

Previous studies have shown that one of the important mechanisms in the magnetic hyperthermia is the tumor inhibition effect of reactive oxygen species (ROS) produced by MNPs through the Fenton reaction (Dai et al. 2019; He et al. 2021; Liu et al. 2020a). It is also noted that the potency of Fenton chemistry is highly dependent on the reaction condition such as reaction temperature (Bossmann et al. 1998). Therefore, a synergism of nanocatalytic therapy and thermal therapy for enlarging ˚OH production is highly desirable at current stage (Su et al. 2015). Motivated by this work, our results of DCF fluorescent showed a significantly higher amount of ROS production by GOSPION nanoparticles compared to the control group ($P < 0.05$, Fig. 5E). Compared to our previous studies conducted on 5-Fu-loaded magnetite/PEG-PCL-PEG-folic acid nanoparticles, these nanoparticles were able to produce a significant amount of ROS ($P < 0.01$) (Mirzaghavami et al. 2021). This enhanced ROS generation can be attributed to graphene oxide (GO) nanosheets (Yang et al. 2015). Pereira et al. and Dai et al. have proven that the Fenton reaction is temperature dependent; this enhancement of ROS production may be attributed to mechanical stress owing to vibration of nanoparticles in AMF (Dai et al. 2019; Pereira et al. 2012).

AST and ALT are the most commonly used biomarkers of hepatocellular injury, liver inflammation, and toxic injury (Ramaiah 2007). All animals had normal ALP levels, indicating that hepatic metabolism was not disturbed by the various treatments (Fig. 7E). However, elevated AST levels were only shown for MH treatment. Because all the glioma-bearing rats survived the experiment, we concluded that the liver had not been seriously been damaged. In addition, mice in the AMF groups did not exhibit increased liver enzymes compared to animals in non-magnetic groups. Therefore, we also concluded that the high-frequency AMF that we applied to the animals had not affected liver function to a significant extent. Hou et al. studies also confirmed that the high-frequency reciprocal magnetic field did not have a significant

effect on the function of the liver and all Balb/c mice with CT-26 colon tumors (Hou et al. 2009).

One of the most important factors for treating rats with magnetic hyperthermia method is the transfer of nanoparticles to the tumor tissue from blood–brain barrier. There are several solutions for this problem, including active and passive targeted delivery. In this study, we used an external magnetic field to induce nanoparticle accumulation in the tumor tissue. As shown in MRI images (Fig. 8A), this method caused more nanoparticles to accumulate on the right side of the tumor area than on the left side. It should be noted that the simultaneous use of a constant magnetic field and smart nanoparticles with ligands such as folic acid (Afzalipour et al. 2021) and transferrin (Wang et al. 2022) can increase the amount of nanoparticles delivered to the tumor tissue compared to the application of the field alone.

In animal studies, rats with glioma tumors were treated in different groups (GOSPIONs, AMF, and MH). The effect of therapeutic methods on glioma rats was evaluated by measuring tumor volume, monitoring of survival rate and apoptosis rate by real-time PCR and Western blotting. According to our results, the performance of the AMF in the animal was much better than the cell such that this enhancement could be due to the effective role of blood hemoglobin and increased blood perfusion in response to hyperthermia (Dai et al. 2019; Mirzaghavami et al. 2021). MH treatment elicited a significant decrease in tumor volume and increased survival of rats compared to other treatment groups (Fig. 8). The additive effects are the result of the combined metabolic effects of nanoparticle, such as production of ROS, and those of hyperthermia, including production of heat via Néelian relaxation. The fact that the tumors did not completely disappear and relapsed suggests that more than one treatment modality (combination chemotherapy or radiotherapy) may be required to achieve a long-term antitumor effect. One important reason is that due to the low intratumoral concentration of nanoparticles, at least in the tumor model used, underdosed temperature zones may occur in some cases.

The ability to induce effective cell death in mild hyperthermia conditions (41 to 43 °C) is generally in the form of apoptotic death (Oh et al. 2016; Qu et al. 2014). Our results regarding the mechanism of apoptotic death both in the cell phase by flow cytometry (Fig. 6) and in the animal phase by molecular methods confirm this issue (Figs. 9 and 10). The live/dead assay findings in Fig. 6 are in good agreement with the results of the MTT assay. Based on Figs. 9 and 10, the highest expression of Bax corresponded to rats treated with MH, and the difference was significantly compared to the other groups ($P < 0.001$), although this value was lower for protein than the gene expression (Fig. 10).

Conclusion

Our results showed that MH treatment (43–44 °C) has the strongest antitumor effect in glioma treatment. Accordingly, this therapy could serve as a promising thermotherapy procedure for the treatment of glioma. Therefore, the advanced GOSPION nanoparticles in this study can be proposed as a promising nanoheater for thermomagnetic cancer treatment by enhancement producing ROS and inducing apoptotic death.

Methods

Synthetized and characterization of MH nanoheaters

SPIONs were synthesized based on chemical co-precipitation method and graphene oxide nanoparticles (NGO) were generated according to the Hummer's method (Shirvalilou et al. 2018). Next, PLGA-coated magnetic graphene oxide (GO/SPIO/PLGA) nanoheaters were synthesized via modified multiple emulsion solvent evaporation. In the first step, 50 mg of synthetized SPIONs (9.6 ± 0.4 nm) was dispersed in 0.5 mL of dichloromethane (DCM) solution in an ultrasonic bath. In the second step, for an inner aqueous solution, 10 mg of NGO was suspended in distilled water (DW), and after that, Tween 60 (15 mg) was added. In the third step, the magnetic dispersion was added to the inner aqueous solution under a sonicator probe. In the fourth step, this mixture was added to an organic solution of 50 mg of PLGA polymer plus 250 mg of Span60 in 6 mL of DCM under sonication. This double emulsion was added to 15 mL of a solution of 150 mg of Tween 60 dissolved in a mixture of 7.5 mL of DW and 7.5 mL of glycerin, and the mixture was sonicated for 30 s. The obtained emulsion was diluted in 12 mL of DW and 12 mL of glycerin while being stirred for 4 h at 25 °C. Finally, the prepared magnetic nanoparticles were centrifuged, washed 3–4 times in DW, and then collected by a permanent magnet. The magnetic nanoparticles were freeze-dried and kept at 4 °C.

Characterization of GOMNPs

The shape of GOSPIO nanoheaters was evaluated by transmission electron microscopy (TEM), hydrodynamic size and surface charge by dynamic light scattering (DLS) and Zetasizer, respectively. DLS measurements were performed with samples dispersed in distilled water in room temperature. 3D shape of magnetic nanoparticles was evaluated through scanning electron microscopy (SEM). Furthermore, evaluation of changes in hydrodynamic size and zeta potential of SPIONs and GOSPIONs were analyzed through DLS. Hysteresis loops (M–H curves) of GOSPIONs were obtained at $T = 300$ K under the magnetic field (up to 15 kOe (by vibrating sample magnetometer (VSM).

Experimental biology methods

After the synthesis and confirmation of the characteristics of nanoparticles, experimental tests were performed in three stages: in vitro, ex vivo and in vivo. Figure 11 shows the schematic of the study methods.

Ex vivo studies

Magnetic guiding with permanent magnets

For in vivo magnetic targeting, we designed and used a device that applies an external force to enhance the accumulation and penetration of GOSPIONs in rat brain tumors. The device consists of two NdFeB permanent magnets with a MH intensity of 1.3 T ($100 \times 50 \times 50$ mm). The magnets were fixed at a distance of 6 cm from each other by the holder. The magnetic density inside the magnetic field phantom (the space between the two blocks) was measured by a Teslameter (LEYBOLD, Germany). In addition, the intensity of the magnetic field between two magnets was simulated by finite element

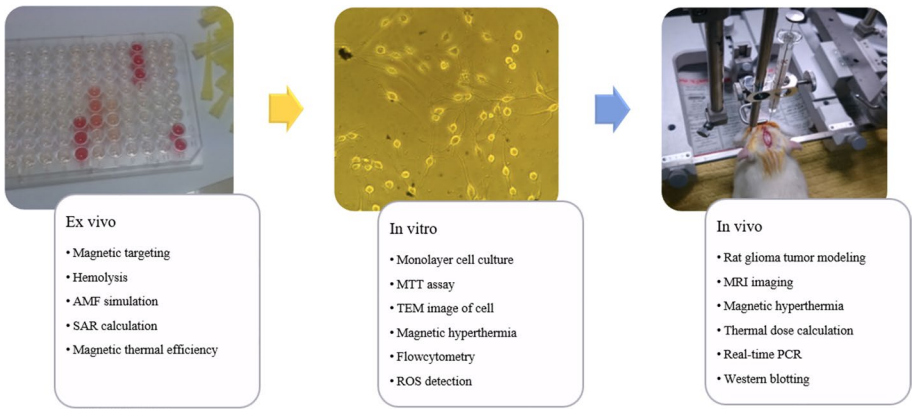

Fig. 11 Flowchart of testing procedures

magnetic field simulation software (Quickfield TM, Fig. 3). Using the data obtained from this simulation, a color map and graphs of the resulting values of the magnetic intensity at the specified locations are illustrated in Fig. 3.

Blood cell hemolytic toxicity

The blood compatibility of GOSPIONs and cytotoxicity effect on healthy male rat erythrocytes (RBCs) were analyzed using a hemolysis test. Erythrocytes were extracted from rat blood samples in heparin-coated tubes and diluted with PBS (4:1). Then GOSPION nanoparticles were added to the blood samples prepared at different concentrations (10 to 4000 µg/mL). All samples were incubated for 2 h at 37 °C with shaking. After 2 min of centrifugation, the supernatant of the samples was collected and transferred to a 96-well plate. Deionized water (DW) and PBS buffer were used as positive and negative controls, respectively. The absorbance of the samples was read at a wavelength of 540 nm by an ELISA reader (BioTek, Winooski, USA). Equation 1 was used to calculate the percentage of hemolysis.

$$\text{Hemolysis}\% = \frac{OD_{\text{sample}} - OD_{\text{PBS}}}{OD_{\text{DW}} - OD_{\text{PBS}}} \times 100. \tag{1}$$

High-frequency induction magnetic heating setup

The alternating magnetic coil (AMC, 13.56 MHz) presented in this work for generating an alternating magnetic field (AMF) is a development of the previously reported iterations in the literature (Mirzaghavami et al. 2022). The current passes through a four-turn water-cooled copper coil with an inner diameter of 40 mm. The coil is placed inside a copper shield. The frequency and field range of the coil used in these experiments were adjusted to fit the accepted ethical limits of the AMF ($Hf = 5.42 \times 108\ Am^{-1}\ s^{-1} < 5 \times 109\ Am^{-1}\ s^{-1}$) (Cho et al. 2017; Mai et al. 2019). This coil was able to generate a high AMF, with acceptable homogeneity, in the space inside the coil where the sample (cell or animal) is placed (Fig. 4B). The distribution of alternating magnetic field inside the coil was simulated with COMSOL Multiphasic 4.3b software and presented as a color map in Fig. 4B. For both in vitro and in vivo experiments, the temperature changes of the

samples inside the coil were monitored by infrared thermal imaging using a Testo (875-2i, UK) infrared camera and thermocouple.

Magnetic nanoparticles as high-frequency nano-heaters

The AMF responsiveness and heating efficiency of the GOSPIONs were estimated by measuring the temperature of the magnetic suspension under applied of the AMF using an AMC. Different concentrations (0, 1, 2, or 3 mg/mL) of GOSPION solutions were transferred into a Petri dish. The Petri dish was placed at the center of an induction copper coil, and an AMF with an output power of 80 W was applied until the temperature of 43 °C was reached to obtain the temperature–time (ΔT/Δt) curves. During heating, temperature changes were monitored with an IR camera. To evaluate the heating efficiency of GOSPIONs as magnetic nanoheaters, the specific absorption rate (SAR, W/g of Fe) was calculated by Eq. 2:

$$\mathrm{SAR} = \frac{C}{m_{Fe}} \times \frac{\Delta T}{\Delta t}. \tag{2}$$

In the above equation, C is the specific heat capacity of water, m is the mass of iron nanoparticles per suspension, and ΔT/Δt is the initial slope of the time-dependent temperature curve. The C of water is 4.18 J/g°C. In addition, the effects of thermal efficiency of GOSPION nanoheaters with "TER times" factor on the temperature elevation rate were determined using the following equation.

$$\mathrm{TER} = \frac{\text{The rate of temperature increase in the presence of nanoparticles}}{\text{The rate of temperature increase in the absence of nanoparticles}}. \tag{3}$$

Furthermore, Kallumadil et al. (2009) introduced the system-independent intrinsic loss power (ILP), as a standard alternative for SAR, which is given in Eq. 4:

$$\mathrm{ILP} = \frac{\mathrm{SAR}}{\mathrm{H}^2 \times \mathrm{f}}, \tag{4}$$

where H is the field strength (AMF) and *f* frequency.

AMF heating profile in culture medium vs blood

To investigate the nanoparticles heating efficiency in vitro and in vivo conditions, suspension of nanoparticles (2 mg/mL) was prepared in culture medium and blood, respectively. The samples were placed inside the coil and the temperature changes were recorded by the IR camera during 20 min.

In vitro experiments

Monolayer C6 and OLN-96 cell cultures

For cell experiments, two types of healthy rat glial (OLN-93) and cancer rat glioblastoma (C6) cells were obtained from Pasteur Cell Bank of Tehran, Iran. C6 and OLN-93 cells were cultured as monolayer in Ham's F-12 and DMEM complete medium (supplemented with 10% fetal bovine serum (FBS), respectively.

In vitro cytotoxicity assay

To assess in vitro cytotoxicity and magnetic nano-heating potential of GOSPIONs, both cells were seeded in a 96-well plate (1×10^4 cells/well) and kept at 37 °C for 24 h. Then the culture mediums were replaced with the mediums containing GOSPIONs in different concentrations (ranging from 0 to 2000 μg/mL) for 24 h. For MH therapy, the cells were placed inside the magnetic coil for 7 min, and during the MH treatment of the cells of the control group, they were kept in an incubator at a temperature of 37 °C. After that, the medium of the wells was removed and the wells were washed with cold FBS, and then MTT solution (5 mg/mL) was added to the wells and incubated for 4 h. After removing MTT, 200 μL of dimethyl sulfoxide (DMSO) was added to the wells and the plate placed on a shaker for 20 min. And finally, the absorbance of the plate was measured at 570 nm by an Elisa reader (BioTek, Winooski, VT). Cell viability was evaluated as the follow equation:

$$\text{Cell viability\%} = \frac{OD_{\text{treated cell}} - OD_{\text{Background}}}{OD_{\text{controlcell}} - OD_{\text{Background}}} \times 100. \tag{5}$$

The following formula was also used to calculate the enhancement therapeutic efficacy of magnetic hyperthermia:

$$\text{Enhancement theraputic efficacy}(\%) = \frac{IC50_{\text{nanoparicle}} - IC50_{MH}}{IC50_{\text{nanoparticle}}} \times 100. \tag{6}$$

Cellular internalization of GOSPION nanoheaters

The C6 cell uptake of GOSPION nanoparticles was confirmed by a TEM image. Cells were incubated with 1.5 mg/mL of GOSPIONs overnight. Then cells were rinsed with PBS buffer and the samples were prepared on a grid, and stained by uranyl acetate and lead citrate staining. The TEM images were obtained by a Zeiss LEO906 (Jena, Germany).

Enhanced ROS generation by GOSPIONs mediated MH

2′,7′-Dichlorofluorescein diacetate (DCFH-DA) agent was used to evaluate the amount of reactive oxygen species (ROS) produced inside the cell during MH. For this purpose, 4×10^5 C6 cells/well were cultured in a 24-well plate, and after 24 h of treatment with nanoparticles (0.5 mg/mL), they were placed inside the coil for hyperthermia (Fig. 4C). After applying the treatment protocol, the culture medium was replaced with DCFH-DA and incubated in the dark condition for 1 h at 37 °C. Then the cells were rinsed and the fluorescent intensity of DCF was measured by an ELISA reader at an excitation wavelength of 485 nm and an emission wavelength of 530 nm.

Mechanism of C6 and OLN-93 cells death under magnetic hyperthermia

C6 and OLN-93 cells were seeded in T-25 flasks at a density of 25×10^4, and kept overnight. Then GOSPIONs (1 mg/mL) were added to the cells and after 24 h; the flasks were exposed to AMF inside the coil until reaching a mean temperature of 43 °C. The time

of being inside the coil for cells treated with nanoheaters and untreated cells was 7 and 25 min, respectively. Finally, the percentage of apoptotic and necrotic cells treated with different methods was evaluated using the Annexin V-FITC/PI I kit (Mabtag, Germany). Cells were trypsinized, counted, and washed with PBS buffer, then a cell suspension of 10^5 cells in 100 µL of ice-cold 1 × attachment buffer was prepared according to the kit manufacturer. After, Annexin V-FITC (about 5 µL) and propidium iodide (PI, 5 µL) were added to 100 µL of the cell suspension, and the mixture was kept at room temperature in the dark. Next, the cells were rinsed with 1 × binding buffer and the fluorescent intensity was immediately assessed using a BD FACS Calibur flow cytometer (BD, San Jose, CA, USA).

In vivo experiments

Animals and ethics

For in vivo studies, male Wistar rats weighing about 180 to 200 g were obtained from the Experimental Research Center of Iran University of Medical Sciences (Tehran, Iran), and were kept under standard conditions in the same center during the experiments. All experiments were performed according to the instructions of the Ethical Committee of Iran University of Medical Sciences (No. IR.IUMS.REC 1400.1125). Also, this project has been accepted by Ethics Committee of Zahedan university of Medical Sciences (Ethic code: IR.ZAUMS.REC.1400.349, Grant No: 10468). (Link: https://ethics.research.ac.ir/EthicsProposalViewEn.php?id=240830).

Liver enzymes assay

Twelve rats were used for the liver enzymes assay. Rats were randomly divided into four groups: saline, MNPs (30 mg/kg), AMF (30 watts, 40 A/m, 30 min), and MH (30 mg/kg MNPs + 15 min under AMF). After 24 h of treatment, the rats were anesthetized with ketamine–xylazine followed by the collection of blood samples the heart. The collected blood samples were put into coagulant tubes. Serum levels of aspartate aminotransferase (AST), and alanine aminotransferase (ALT) were measured by standard enzymatic method using a Vitros 250 analyzer (Ortho-Clinical-Diagnostics; Raritan, NJ, USA).

In vivo allograft glioma tumor model

Animals were anesthetized by intravenous injection of ketamine/xylazine combination (75 mg/kg and 5 mg/kg). Anesthetized mice were immobilized on a stereotactic frame, and a 1 mm hole was made in their skull (2 mm anterior, + 2 mm lateral, and 4 mm deep). After that, one million C6 glioma cells were prepared in 10 µl culture medium and injected into the brains of rats by a Hamilton syringe at a speed of 2 µL/min. MRI imaging was used to diagnose tumor formation and calculate tumor volume.

Evaluating the glioma tumor with MRI imaging

All T2-weighted MRI images of the rat brain were obtained by a 3 T MAGNETOM Prisma scanner (Siemens, Germany) with a rat head coil with a turbo-spin-echo protocol. The imaging protocol as reported in the previous study was equal to (Shirvalilou et al. 2018): TR = 2300 ms, TE = 107 ms; NEX = 3; matrix size = 256 × 256;

FOV = 47 mm × 47 mm; slice thickness = 1 mm and number of slices = 20. Finally, ITK-SNAP 3.4 software was used for image analysis and tumor volume calculation.

Antitumor effects of GOSPIONs mediated MH on glioma-bearing tumor

Forty rats were subjected to MRI imaging 13 days after tumor implantation to confirm tumor formation, and rats whose tumor volume was between 50 and 100 mm^3 were randomly distributed into four groups, each group containing 9 rats. We tried to minimize the difference in tumor size in each group. The groups were Group 1: normal saline (sham), Group 2: GOSPIONs alone, Group 3: Alternating magnetic field (AMF) alone, Group 4: magnetic hyperthermia (MH; AMF + GOSPIONs).

On day 14, all animals were anesthetized to start treatment and then treated with the following protocol.

G1: saline buffer was injected intravenously into the tail of rat.

G2: GOSPION nanoparticles were administered into the tail vein of rat at a dose of 30 mg/kg and the rats were subjected to a permanent magnetic field for 2 h.

G3: The rat's head was placed inside the coil (30 watts, 40 A/m) for 30 min (Fig. 7). The time of 30 min was calculated based on the thermometric curve of the rat by the IR camera.

G4: First, nanoparticles were injected, and the rat's head was placed in a constant magnetic field phantom for targeted transmission for 1 h, and then it was placed inside the coil for 15 min for magnetic hyperthermia.

For groups 3 and 4, the treatment protocol was repeated for 3 consecutive days. 2 h after receiving the last treatment, 3 rats from each group were killed and the brain tissue of the rats was extracted to check the level of gene and protein expression by Real time PCR and Western blotting assay, respectively. Another 6 rats in each group were followed to evaluate the survival time, body weight and the tumor volume changes.

Heating profile and thermal dose generated by AMF

For MH therapy, the time–temperature curve was drawn to determine the time required for the rats to be inside the coil to reach a mean temperature of 43–44 °C. For magnetic hyperthermia treatment, a temperature–time curve was drawn to determine the time required for mice to be inside the coil to reach an average temperature of 43–44 °C. The heads of mice bearing glioma with and without nanoparticle injection were placed inside the coil and exposed to AMF. For this purpose, glioma-bearing rats' heads with and without nanoparticle injection were placed inside the coil and exposed to AMF (13.56 MHz, 30 W) and temperature changes were monitored by a IR camera. Using heat maps obtained during MH treatment, an ROI was drawn around each tumor to extract temperature data at each pixel. Then according to Sapareto and Dewey 1984 (Dewey et al. 1977), the cumulative equivalent minute thermal dose at 43 °C (CEM 43 °C) was estimated as follows:

$$\mathrm{CEM43^{\circ}C} = \sum_{i=1}^{n} t(i)\mathrm{R}^{[43-T(i)]}. \tag{7}$$

In this equation, $t(i)$ is the time interval of (i)th sample, $T(i)$ is the average temperature in a certain time interval of heating at the (i)th minute. The R constant is 1/4 and 1/2 for lower and higher temperatures than 43 °C, respectively.

Gene expression study using real-time PCR

Mild hyperthermia can induce apoptosis, for this reason, to investigate the mechanism of death caused by hyperthermia treatment, the expression levels of apoptosis inducing (Bax) and inhibiting genes (Bcl-2) were investigated by real-time PCR method. First, according to the instructions of the kit (Takara, Japan), total RNA was extracted from tumor tissue (approximately 30 mg). The concentration and purity of the extracted RNA was determined through Nano-drop spectrophotometer (Thermo Scientific, USA), and cDNA was synthesized according to the cDNA kit (Yekta tajhiz, Yetco, Tehran, Iran). Then, according to the instructions of the YTA SYBR Green qPCR MasterMix 2X (Yekta tajhiz, Iran), the materials were prepared and transferred to real-time PCR StepOne plus (Applied Biosystems, USA). GAPDH gene was used as housekeeping gene, and the PCR results were normalized to GAPDH. The sequences of primers used are reported in Table 3.

Protein expression study using Western blotting analysis

The expression of Bax and Bcl2 proteins in glioma-bearing rats was investigated using Western blotting method. Tumor tissue was extracted, homogenized, and then total protein was extracted by RIPA lysis buffer (Santa Cruz Biotechnology, Dallas, USA). The extracted protein was quantified by the Bradford protein assay. The primary antibodies Bax (ABclonal Company, USA, 1:500), Bcl-2 (ABclonal Company, USA, 1:1000) and β-actin (ABclonal Company, USA, 1:500), and horseradish peroxidase (HRP) conjugated-secondary antibody (ABclonal Company, USA, 1/2000) was used for Western blotting assay. Protein bands were observed using western blotting Chemiluminescent reagent (ChemiDocXRS; South San Francisco, USA), and analyzed using ImageJ.

Statistical analysis

All experiments were performed at least 3 times, and data reported as mean ± standard deviation. The statistical analysis of the data was assessed for significance by one-way analysis of variance (ANOVA) followed by Tukey's test by GraphPad Prism 6 software. A $P < 0.05$ or lower was considered to be statistically significant (marked by *).

Abbreviations

MH	Magnetohyperthermia
AMF	Alternating magnetic field
SPIONs	Superparamagnetic nanoparticles
GO	Graphene oxide
AMC	Alternating magnetic coil
SAR	Specific absorption rate
CEM 43 °C	Cumulative equivalent minute 43 °C

Acknowledgements

We thank the National Brain Mapping Laboratory of Iran for providing the MR imaging and technical assistance at all steps of the experimental studies.

Author contributions

All authors contributed to the study conception and design. Prof. Sepideh Khoee and Dr. MSh contributed to material preparation.Dr. RSh, MG, Dr. SSh, Prof. SKhoei and ES conducted the experiments and collected the data. The first draft

of the manuscript was written by Dr. RSh and Dr. SSh. All the authors reviewed the manuscript. All aspects of the study were supervised by Prof. SKhoei, and Dr. SSh. All authors read and approved the final manuscript.

Funding
This work was supported by a Grant No. 21798 from Iran University of Medical Sciences (IUMS). This project financially has been supported by Zahedan university of Medical Sciences (Ethic code: IR.ZAUMS.REC.1400.349, Grant No: 10468). (Link: https://ethics.research.ac.ir/EthicsProposalViewEn.php?id=240830).

Availability of data and materials
The datasets used and/or analyzed during the current study are available from the corresponding author on reasonable request.

Declarations

Ethics approval and consent to participate
This research was approved by Ethics Committee of Iran University of Medical Sciences. Animal cell lines used in this study do not require ethics approval.

Consent for publication
Not applicable.

Competing interests
The authors have no competing interests.

Received: 22 November 2022 Accepted: 4 April 2023
Published online: 26 April 2023

References

Afzalipour R, Khoei S, Khoee S, Shirvalilou S, Raoufi NJ, Motevalian M, Karimi MY (2021) Thermosensitive magnetic nanoparticles exposed to alternating magnetic field and heat-mediated chemotherapy for an effective dual therapy in rat glioma model Nanomedicine: nanotechnology. Biol Med 31:102319
Asadi L, Shirvalilou S, Khoee S, Khoei S (2018) Cytotoxic effect of 5-fluorouracil-loaded polymer-coated magnetite nanographene oxide combined with radiofrequency. Anti-Cancer Agents Med Chem 18:1148–1155
Belanova AA, Gavalas N, Makarenko YM, Belousova MM, Soldatov AV, Zolotukhin PV (2018) Physicochemical properties of magnetic nanoparticles: implications for biomedical applications in vitro and in vivo. Oncol Res Treat 41:139–143
Beola L, Asín L, Fratila RM, Herrero V, De La Fuente JM, Grazú V, Gutiérrez L (2018) Dual role of magnetic nanoparticles as intracellular hotspots and extracellular matrix disruptors triggered by magnetic hyperthermia in 3D cell culture models. ACS Appl Mater Interfaces 10:44301–44313
Berkovitch M et al (2000) The efficacy of oral deferiprone in acute iron poisoning. Am J Emerg Med 18:36–40
Bossmann SH et al (1998) New evidence against hydroxyl radicals as reactive intermediates in the thermal and photochemically enhanced Fenton reactions. J Phys Chem A 102:5542–5550
Bychkova A, Sorokina O, Rosenfeld M, Kovarski A (2012) Multifunctional biocompatible coatings on magnetic nanoparticles. Russ Chem Rev 81:1026
Chen R, Christiansen MG, Anikeeva P (2013) Maximizing hysteretic losses in magnetic ferrite nanoparticles via model-driven synthesis and materials optimization. ACS Nano 7:8990–9000
Cho M et al (2017) Assembly of iron oxide nanocubes for enhanced cancer hyperthermia and magnetic resonance imaging. Nanomaterials 7:72
Clogston JD, Patri AK (2011) Zeta potential measurement. In: McNeil S (ed) Characterization of nanoparticles intended for drug delivery. Springer, Berlin, pp 63–70
Dai C et al (2019) Photonic/magnetic hyperthermia-synergistic nanocatalytic cancer therapy enabled by zero-valence iron nanocatalysts. Biomaterials 219:119374
de Escalona MM, Sáez-Fernández E, Prados JC, Melguizo C, Arias JL (2016) Magnetic solid lipid nanoparticles in hyperthermia against colon cancer. Int J Pharm 504:11–19
Dewey W, Hopwood L, Sapareto S, Gerweck L (1977) Cellular responses to combinations of hyperthermia and radiation. Radiology 123:463–474
Di Corato R et al (2014) Magnetic hyperthermia efficiency in the cellular environment for different nanoparticle designs. Biomaterials 35:6400–6411
Eivazzadeh-Keihan R et al (2022) Magnetic graphene oxide–lignin nanobiocomposite: a novel, eco-friendly and stable nanostructure suitable for hyperthermia in cancer therapy. RSC Adv 12:3593–3601
El-Dek S, Ali MA, El-Zanaty SM, Ahmed SE (2018) Comparative investigations on ferrite nanocomposites for magnetic hyperthermia applications. J Magn Magn Mater 458:147–155
Giannini EG, Testa R, Savarino V (2005) Liver enzyme alteration: a guide for clinicians. CMAJ 172:367–379
Gilchrist R, Medal R, Shorey WD, Hanselman RC, Parrott JC, Taylor CB (1957) Selective inductive heating of lymph nodes. Ann Surg 146:596
Greish K (2010) Enhanced permeability and retention (EPR) effect for anticancer nanomedicine drug targeting. In: Grobmyer SR, Moudgil BM (eds) Cancer nanotechnology. Springer, Berlin, pp 25–37
Gu Y et al (2020) Magnetic hyperthermia with e-Fe2O3 nanoparticles
Hatamie S, Balasi ZM, Ahadian MM, Mortezazadeh T, Shams F, Hosseinzadeh S (2021) Hyperthermia of breast cancer tumor using graphene oxide-cobalt ferrite magnetic nanoparticles in mice. J Drug Deliv Sci Technol 65:102680

He Y, Yi C, Zhang X, Zhao W, Yu D (2021) Magnetic graphene oxide: synthesis approaches, physicochemical characteristics, and biomedical applications. TrAC Trends Anal Chem 136:116191
Hilger I, Hergt R, Kaiser WA (2005) Towards breast cancer treatment by magnetic heating. J Magn Magn Mater 293:314–319
Hou C-H, Hou S-M, Hsueh Y-S, Lin J, Wu H-C, Lin F-H (2009) The in vivo performance of biomagnetic hydroxyapatite nanoparticles in cancer hyperthermia therapy. Biomaterials 30:3956–3960
Iyer AK, Khaled G, Fang J, Maeda H (2006) Exploiting the enhanced permeability and retention effect for tumor targeting. Drug Discovery Today 11:812–818
Jahangiri S, Khoei S, Khoee S, Safa M, Shirvalilou S, Pirhajati Mahabadi V (2021) Potential anti-tumor activity of 13.56 MHz alternating magnetic hyperthermia and chemotherapy on the induction of apoptosis in human colon cancer cell lines HT29 and HCT116 by up-regulation of Bax, cleaved caspase 3&9, and cleaved PARP proteins. Cancer Nanotechnol 12:1–17
Jang JT, Nah H, Lee JH, Moon SH, Kim MG, Cheon J (2009) Critical enhancements of MRI contrast and hyperthermic effects by dopant-controlled magnetic nanoparticles. Angew Chem Int Ed 48:1234–1238
Jeon S et al (2020) Heat-generating iron oxide multigranule nanoclusters for enhancing hyperthermic efficacy in tumor treatment. ACS Appl Mater Interfaces 12:33483–33491
Johannsen M, Thiesen B, Wust P, Jordan A (2010) Magnetic nanoparticle hyperthermia for prostate cancer. Int J Hyperth 26:790–795
Kalamida D, Karagounis IV, Mitrakas A, Kalamida S, Giatromanolaki A, Koukourakis MI (2015) Fever-range hyperthermia vs hypothermia effect on cancer cell viability, proliferation and HSP90 expression. PLoS ONE 10:e0116021
Kallumadil M, Tada M, Nakagawa T, Abe M, Southern P, Pankhurst QA (2009) Suitability of commercial colloids for magnetic hyperthermia. J Magn Magn Mater 321:1509–1513
Kargar S, Khoei S, Khoee S, Shirvalilou S, Mahdavi SR (2018) Evaluation of the combined effect of NIR laser and ionizing radiation on cellular damages induced by IUdR-loaded PLGA-coated nano-graphene oxide. Photodiagnosis Photodyn Ther 21:91–97
Karimipour K, Rad JK, Shirvalilou S, Khoei S, Mahdavian AR (2021) Spiropyran-based photoswitchable acrylic nanofibers: a stimuli-responsive substrate for light controlled C6 glioma cells attachment/detachment. Coll Surf B Biointerfaces 203:111731
Kumar R, Chauhan A, Jha SK, Kuanr BK (2018) Localized cancer treatment by radio-frequency hyperthermia using magnetic nanoparticles immobilized on graphene oxide: from novel synthesis to in vitro studies. J Mater Chem B 6:5385–5399
Lanier OL et al (2019) Evaluation of magnetic nanoparticles for magnetic fluid hyperthermia. Int J Hyperth 36:686–700
Li T et al (2015) Polyetherimide-grafted Fe3O4@ SiO2 nanoparticles as theranostic agents for simultaneous VEGF siRNA delivery and magnetic resonance cell imaging. Int J Nanomed 10:4279
Liu XL, Fan HM, Yi JB, Yang Y, Choo ESG, Xue JM, Ding J (2012) Optimization of surface coating on Fe_3O_4 nanoparticles for high performance magnetic hyperthermia agents. J Mater Chem 22:8235–8244
Liu X et al (2020a) Graphene oxide-grafted magnetic nanorings mediated magnetothermodynamic therapy favoring reactive oxygen species-related immune response for enhanced antitumor efficacy. ACS Nano 14:1936–1950
Liu X et al (2020b) Comprehensive understanding of magnetic hyperthermia for improving antitumor therapeutic efficacy. Theranostics 10:3793
Mai BT et al (2019) Thermoresponsive iron oxide nanocubes for an effective clinical translation of magnetic hyperthermia and heat-mediated chemotherapy. ACS Appl Mater Interfaces 11:5727–5739
Mirzaghavami PS, Khoei S, Khoee S, Shirvalilou S, Mahdavi SR, Mahabadi VP (2021) Radio-sensitivity enhancement in HT29 cells through magnetic hyperthermia in combination with targeted nano-carrier of 5-Flourouracil. Mater Sci Eng C 124:112043
Mirzaghavami PS, Khoei S, Khoee S, Shirvalilou S (2022) Folic acid-conjugated magnetic triblock copolymer nanoparticles for dual targeted delivery of 5-fluorouracil to colon cancer cells. Cancer Nanotechnol 13:1–18
Mohammadi S, Khoei S, Mahdavi SR (2012) The combination effect of poly (lactic-co-glycolic acid) coated iron oxide nanoparticles as 5-fluorouracil carrier and X-ray on the level of DNA damages in the DU 145 human prostate carcinoma cell line. J Bionanosci 6:23–27
Oei A, Vriend L, Krawczyk P, Horsman M, Franken N, Crezee J (2017) Targeting therapy-resistant cancer stem cells by hyperthermia. Int J Hyperth 33:419–427
Oghabian M, Jeddi-Tehrani M, Zolfaghari A, Shamsipour F, Khoei S, Amanpour S (2011) Detectability of Her2 positive tumors using monoclonal antibody conjugated iron oxide nanoparticles in MRI. J Nanosci Nanotechnol 11:5340-5344·
Oh Y, Lee N, Kang HW, Oh J (2016) In vitro study on apoptotic cell death by effective magnetic hyperthermia with chitosan-coated MnFe2O4. Nanotechnology 27:115101
Pereira M, Oliveira L, Murad E (2012) Iron oxide catalysts: Fenton and Fentonlike reactions–a review. Clay Miner 47:285–302
Périgo EA, Hemery G, Sandre O, Ortega D, Garaio E, Plazaola F, Teran FJ (2015) Fundamentals and advances in magnetic hyperthermia applied. Phys Rev 2:041302
Piazza RD et al (2020) Peglatyon-SPION surface functionalization with folic acid for magnetic hyperthermia applications. Mater Res Express 7:015078
Qu Y, Li J, Ren J, Leng J, Lin C, Shi D (2014) Enhanced magnetic fluid hyperthermia by micellar magnetic nanoclusters composed of Mn x Zn1–x Fe2O4 nanoparticles for induced tumor cell apoptosis. ACS Appl Mater Interfaces 6:16867–16879
Ramaiah SK (2007) A Toxicologist guide to the diagnostic interpretation of hepatic biochemical parameters. Food Chem Toxicol 45:1551–1557
Rego GN et al (2020) Therapeutic efficiency of multiple applications of magnetic hyperthermia technique in glioblastoma using aminosilane coated iron oxide nanoparticles: in vitro and in vivo study. Int J Mol Sci 21:958

Rodrigo I et al (2020) Exploring the potential of the dynamic hysteresis loops via high field, high frequency and temperature adjustable AC magnetometer for magnetic hyperthermia characterization International. J Hyperth 37:976–991
Roizin-Towle L, Pirro JP (1991) The response of human and rodent cells to hyperthermia International. J Radiat Oncol Biol Phys 20:751–756
Salopek B, Krasic D, Filipovic S (1992) Measurement and application of zeta-potential. Rudarsko-Geolosko-Naftni Zbornik 4:147
Shaterabadi Z, Nabiyouni G, Soleymani M (2018) Physics responsible for heating efficiency and self-controlled temperature rise of magnetic nanoparticles in magnetic hyperthermia therapy. Prog Biophys Mol Biol 133:9–19
Shirvalilou S, Khoei S, Khoee S, Raoufi NJ, Karimi MR, Shakeri-Zadeh A (2018) Development of a magnetic nano-graphene oxide carrier for improved glioma-targeted drug delivery and imaging: in vitro and in vivo evaluations. Chem Biol Interact 295:97–108
Shirvalilou S, Khoei S, Khoee S, Mahdavi SR, Raoufi NJ, Motevalian M, Karimi MY (2020) Enhancement radiation-induced apoptosis in C6 glioma tumor-bearing rats via pH-responsive magnetic graphene oxide nanocarrier. J Photochem Photobiol B Biol 205:111827
Shirvalilou S, Khoei S, Esfahani AJ, Kamali M, Shirvaliloo M, Sheervalilou R, Mirzaghavami P (2021) Magnetic hyperthermia as an adjuvant cancer therapy in combination with radiotherapy versus radiotherapy alone for recurrent/progressive glioblastoma: a systematic review. J Neurooncol 152:419–428
Spirou SV, Basini M, Lascialfari A, Sangregorio C, Innocenti C (2018) Magnetic hyperthermia and radiation therapy: radiobiological principles and current practice. Nanomaterials 8:401
Su Y-L, Fang J-H, Liao C-Y, Lin C-T, Li Y-T, Hu S-H (2015) Targeted mesoporous iron oxide nanoparticles-encapsulated perfluorohexane and a hydrophobic drug for deep tumor penetration and therapy. Theranostics 5:1233
Sugumaran PJ, Liu X-L, Herng TS, Peng E, Ding J (2019) GO-functionalized large magnetic iron oxide nanoparticles with enhanced colloidal stability and hyperthermia performance. ACS Appl Mater Interfaces 11:22703–22713
Tong S, Quinto CA, Zhang L, Mohindra P, Bao G (2017) Size-dependent heating of magnetic iron oxide nanoparticles. ACS Nano 11:6808–6816
Umar AA, Patah MFA, Abnisa F, Daud WMAW (2020) Preparation of magnetized iron oxide grafted on graphene oxide for hyperthermia application. Rev Chem Eng. https://doi.org/10.1515/revce-2020-0001
Umar AA, Patah MFA, Abnisa F, Daud WMAW (2021) Rational design of PEGylated magnetite grafted on graphene oxide with effective heating efficiency for magnetic hyperthermia application. Colloids Surf A 619:126545
Vilas-Boas V, Carvalho F, Espiña B (2020) Magnetic hyperthermia for cancer treatment: main parameters affecting the outcome of in vitro and in vivo studies. Molecules 25:2874
Wang QX, Chen X, Li ZL, Gong YC, Xiong XY (2022) Transferrin/folate dual-targeting Pluronic F127/poly (lactic acid) polymersomes for effective anticancer drug delivery Journal of Biomaterials Science. Polymer Edition 33:1140–1156
Xu H, Pan Y (2019) Experimental evaluation on the heating efficiency of magnetoferritin nanoparticles in an alternating magnetic field. Nanomaterials 9:1457
Yang X et al (2015) Fabrication of P25/Ag3PO4/graphene oxide heterostructures for enhanced solar photocatalytic degradation of organic pollutants and bacteria. Appl Catal B Environ 166:231–240
Youhannayee M et al (2019) Physical characterization and uptake of iron oxide nanoparticles of different prostate cancer cells. J Magn Magn Mater 473:205–214
Zeng L et al (2019) Role of protein corona in the biological effect of nanomaterials: investigating methods. TrAC Trends Anal Chem 118:303–314

Publisher's Note